LANGMUIR Article
Cite This: Langmuir 2019, 35, 10658−10666
pubs.acs.org/Langmuir

Influence of NaCl Concentration on Bicelle-Mediated SLB Formation

Tun Naw Sut,[†] Joshua A. Jackman,[‡] Bo Kyeong Yoon,[†] Soohyun Park,[†] Kavoos Kolahdouzan,[§] Gamaliel Junren Ma,[†] Vladimir P. Zhdanov,[∥] and Nam-Joon Cho*[,†,⊥]

[†]School of Materials Science and Engineering, Nanyang Technological University, 50 Nanyang Avenue 639798, Singapore
[‡]School of Chemical Engineering, Sungkyunkwan University, Suwon 16419, Republic of Korea
[§]Department of Chemistry, Pomona College, 645 North College Avenue, Claremont, California 91711, United States
[∥]Boreskov Institute of Catalysis, Russian Academy of Sciences, Novosibirsk 630090, Russia
[⊥]School of Chemical and Biomedical Engineering, Nanyang Technological University, 62 Nanyang Drive 637459, Singapore

Supporting Information

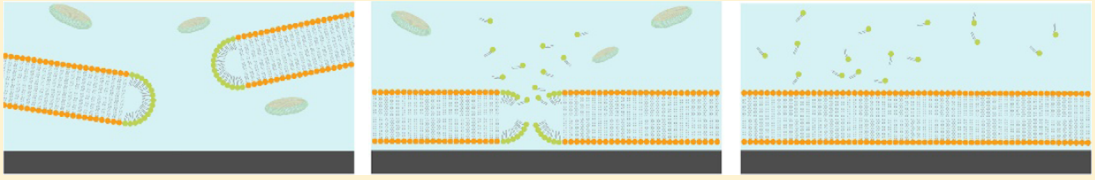

ABSTRACT: The deposition of two-dimensional bicellar disks on hydrophilic surfaces is an emerging approach to fabricate supported lipid bilayers (SLBs) that requires minimal sample preparation, works at low lipid concentrations, and yields high-quality SLBs. While basic operating steps in the fabrication protocol mimic aspects of the conventional vesicle fusion method, lipid bicelles and vesicles have distinct architectural properties, and understanding how experimental parameters affect the efficiency of bicelle-mediated SLB formation remains to be investigated. Herein, using the quartz crystal microbalance-dissipation and localized surface plasmon resonance techniques, we investigated the effect of bulk NaCl concentration on bicelle-mediated SLB formation on silicon dioxide surfaces. For comparison, similar experiments were conducted with vesicles as well. In both cases, SLB formation was observed to occur rapidly provided that the NaCl concentration was sufficiently high (>50 mM). Under such conditions, the effect of NaCl concentration on SLB formation was minor in the case of bicelles and significant in the case of vesicles where it is expected to be related primarily to osmotic pressure. At lower NaCl concentrations, bicelles also formed SLBs but slowly, whereas adsorbed vesicles remained intact. These findings were complemented by time-lapsed fluorescence microscopy imaging and fluorescence recovery after photobleaching measurements that corroborated bicelle-mediated SLB formation across the range of tested NaCl concentrations. The results are discussed by comparing the architectural properties of bicelles and vesicles along with theoretical analysis of the corresponding adsorption kinetics.

INTRODUCTION

Supported lipid bilayers (SLBs) are a cell-membrane-mimicking platform that consists of a two-dimensional lipid bilayer coating[1] and can be integrated with surface-sensitive measurement techniques for sensing applications.[2] SLBs are a promising example of nanoarchitectonics, whereby bottom-up nanofabrication and molecular self-assembly are integrated to build higher-order biomimetic systems.[3,4] At present, the most popular method to form SLBs involves the adsorption and spontaneous rupture of lipid vesicles, a process that is termed "vesicle fusion" and works on certain solid supports such as silicon dioxide-based materials.[5] Depending on the vesicle−substrate interaction strength, SLB formation can occur when individual, adsorbed vesicles rupture upon adsorption (due to sufficiently strong vesicle−substrate interactions) or when adsorbed vesicles reach a critical surface coverage (due to a combination of vesicle−substrate and vesicle−vesicle interactions).[6] In other cases with weaker vesicle−substrate interactions, intact vesicle adsorption without rupture and negligible vesicle adsorption can occur. On a given solid support, the specific adsorption pathway is sensitive to the experimental conditions such as vesicle properties (size, composition, concentration, lamellarity, osmotic pressure), solution environment (solution pH, ionic strength, ion type), and operating parameters (temperature, flow rate) (see, e.g., ref 7 and references therein). Thus, there has been interest in developing alternative SLB fabrication strategies that are more versatile due to simpler preparation protocols and greater robustness to different experimental conditions (see, e.g., ref 8 and references therein).

One promising strategy involves depositing bicellar suspensions, which are composed of a mixture of long-chain and short-chain phospholipids. The lipid mixtures can self-assemble into a variety of morphological structures depending on parameters such as the q-value (ratio of long-chain to short-chain phospholipids), total lipid concentration, and temper-

Received: May 31, 2019
Revised: July 16, 2019
Published: July 18, 2019

DOI: 10.1021/acs.langmuir.9b01644
Langmuir 2019, 35, 10658−10666

ature. Under typical conditions, bicelles are classically viewed as two-dimensional bicellar disks that have proven useful for structural biology studies involving membrane proteins.[9,10] Zeineldin et al. first demonstrated SLB formation on silicon dioxide surfaces from lipid bicelles comprising long-chain 1,2-dipalmitoyl-*sn*-glycero-3-phosphocholine and short-chain 1,2-diheptanoyl-*sn*-glycero-3-phosphocholine ($DHPC_7$) lipids.[11] Tabaei et al. also showed that lipid bicelles composed of dimyristoylphosphatidylcholine and 1,2-dihexanoyl-*sn*-glycero-3-phosphocholine ($DHPC_6$, referred to as DHPC in the following text) can form SLBs on a silicon dioxide substrate as well.[12]

These proof-of-concept studies were followed by more detailed investigations of how varying the q-ratio affects SLB formation on silicon dioxide surfaces from bicellar mixtures composed of zwitterionic 1-palmitoyl-2-oleol-*sn*-glycero-3-phosphocholine (POPC) and short-chain DHPC lipids.[13] More recently, we systematically investigated how total lipid concentration and q-ratio affect SLB formation on silicon dioxide surfaces from bicelles composed of zwitterionic 1,2-dioleoyl-*sn*-glycero-3-phosphocholine (DOPC) and DHPC lipids.[14] Our findings showed that, as expected, bicelle adlayers have distinct mass and viscoelastic properties compared to vesicle adlayers, while also revealing mechanistic insights and demonstrating that the bicelle-mediated SLB formation efficiency is improved at lower lipid concentrations. The latter result was a striking observation that contrasts with previously reported results that have been obtained by the vesicle fusion method and other alternative options such as the solvent-assisted lipid bilayer method.[8] Moreover, we also identified that charged lipid bicelles adsorb onto different oxide surfaces in a manner that is distinct from that of lipid vesicles and likely related to the greater membrane−substrate contact area of adsorbing bicelles.[15] From a physicochemical perspective, such findings motivate further exploration of other experimental conditions such as NaCl concentration in the bulk solution that has been shown to have significant influences on vesicle-mediated SLB formation, including either inhibiting or promoting spontaneous rupture of adsorbed vesicles on silicon dioxide surfaces.[7] Physically, the effect of bulk NaCl concentration on vesicle adsorption and rupture can be related to the deformation of vesicles due to Na^+ and Cl^- ion-induced osmotic pressure effects as well as ion-related electrostatic effects (e.g., charge shielding). Comparing the predictions of the corresponding models (membrane elasticity versus DLVO-type interactions) with the experimental data obtained for zwitterionic POPC lipid vesicles, the influence of osmotic pressure was concluded to be more important.[7] In turn, bicelles can be viewed as nearly close-packed lipid disks and osmotic pressure cannot change the shape of such disks. From this perspective, the effect of osmotic pressure on bicelle rupture is expected to be negligible. On the other hand, NaCl-related electrostatic effects can be operative. Thus, understanding the influence of NaCl concentration on bicelle-mediated SLB formation on silicon dioxide surfaces would provide fundamental knowledge about the bicelle adsorption process as well as offer practical utility for comparing the versatility and robustness of bicelle-mediated SLB formation under different operating conditions.

Toward this goal, herein, we investigated the effect of bulk NaCl concentration on DOPC/DHPC lipid bicelle-mediated SLB formation on silicon dioxide surfaces. The experimental strategy is outlined in Figure 1. By varying this concentration,

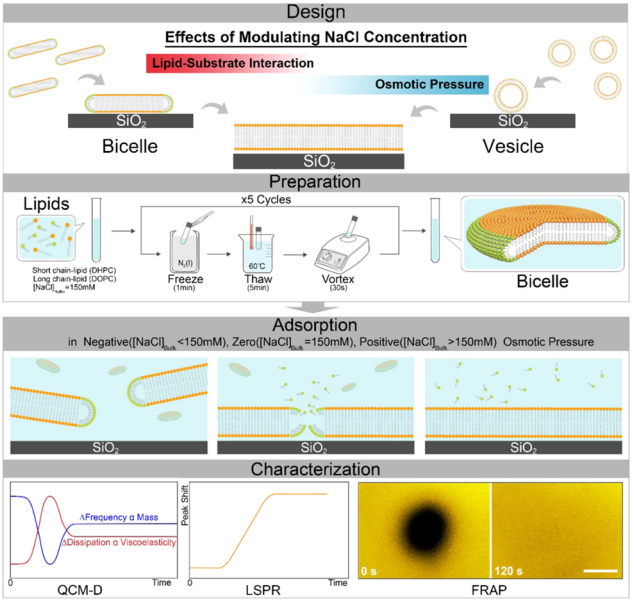

Figure 1. Overview of experimental strategy. We focused on characterizing the effects of NaCl concentration on bicelle adsorption, and we also scrutinized vesicle adsorption in parallel. Bicelle preparation involved a simple protocol that entails hydrating a dry lipid film, followed by five cycles of freeze−thaw−vortexing. Bicelle adsorption was then studied under different NaCl concentrations so that the corresponding osmotic pressure was negative, zero, or positive, and different measurement techniques were applied to characterize the mass, viscoelastic, and morphological properties of the fabricated lipid adlayers.

it was possible to characterize DOPC/DHPC lipid bicelle adsorption and rupture under a variety of positive and negative osmotic pressure conditions along with comparative measurements on equivalently prepared DOPC lipid vesicles. Quartz crystal microbalance-dissipation (QCM-D) and localized surface plasmon resonance (LSPR) biosensing experiments tracked real-time changes in adsorption-related mass, viscoelastic, and conformational properties, whereas time-lapsed fluorescence microscopy imaging aided morphological characterization along with fluorescence recovery after photobleaching (FRAP) measurements for evaluating lateral lipid mobility. These different measurement techniques are complementary, and the advantage of the LSPR technique, for example, is that the corresponding signal is highly sensitive to the conformational properties of an adsorbed lipid structure in the near vicinity of the solid−liquid interface[16] (the earlier NaCl-related results for small, extruded POPC lipid vesicles[7] were obtained using the QCM-D technique alone). Theoretical analysis of the adsorption kinetics corresponding to lipid bicelle and vesicle cases complements the experimental findings, and the results demonstrate that bicelles are robust tools for achieving successful SLB formation across a wide range of NaCl concentrations.

MATERIALS AND METHODS

Reagents. 1,2-Dioleoyl-*sn*-glycero-3-phosphocholine (DOPC), 1,2-dihexanoyl-*sn*-glycero-3-phosphocholine (DHPC), and 1,2-dioleoyl-*sn*-glycero-3-phosphoethanolamine-*N*-(lissamine rhodamine B sulfonyl) (Rh-PE) lipids dispersed in chloroform were obtained from Avanti Polar Lipids (Alabaster, AL). Aqueous buffer solutions were prepared using Milli-Q-treated water (>18 MΩ cm) (MilliporeSigma, Burlington, MA).

DOI: 10.1021/acs.langmuir.9b01644
Langmuir 2019, 35, 10658−10666

Preparation of Lipid Bicelles and Vesicles. Bicellar suspensions were prepared by lipid hydration followed by freeze−thaw−vortexing, as previously described.[14] An aliquot from an as-supplied chloroform solution of long-chain DOPC phospholipids was added to a glass vial to achieve the desired molar ratio and then the chloroform solvent was evaporated by air-blowing with nitrogen gas, resulting in a dry lipid film on the walls of a glass vial. The lipid film was then stored overnight in a vacuum desiccator to remove trace residues of chloroform, followed by subsequent hydration in a DHPC lipid-containing aqueous buffer solution comprising 10 mM Tris (pH 7.5) and 150 mM NaCl. The resulting lipid suspension had a long-chain phospholipid concentration of 1 mM and a q-ratio of 0.25. The lipid suspensions were next treated with five cycles of freeze−thaw−vortex cycling that involved the following steps: submersion in liquid nitrogen for 1 min, thawing in a 60 °C water bath for 5 min, and vortexing for 30 s. The resulting suspension was visually clear at room temperature. Immediately before the experiment, an aliquot of the stock lipid suspension was diluted ∼32-fold using an aqueous buffer solution comprising 10 mM Tris (pH 7.5) with the appropriate NaCl concentration (between 0 and 500 mM NaCl) so that the final long-chain phospholipid concentration was 0.031 mM. An identical protocol was used for preparing DOPC lipid vesicles, except that the dry DOPC lipid film was hydrated in an aqueous buffer solution that did not contain DHPC lipid. According to dynamic light scattering measurements, the lipid bicelles and vesicles had mean diameters around 470 and 300 nm, respectively.

Quartz Crystal Microbalance-Dissipation (QCM-D). Bicelle and vesicle adsorption experiments were conducted using a Q-Sense E4 instrument (Biolin Scientific AB, Stockholm, Sweden). The quartz crystal sensor chips had a fundamental frequency of 5 MHz, and the sensor surface had a 50-nm thick sputter-coated, silicon dioxide layer. Before the experiment, the sensor chips were cleaned by repeatedly washing them with ethanol and water, followed by nitrogen gas drying and then treatment in an oxygen plasma chamber (PDC-002, Harrick Plasma, Ithaca, NY) for 1 min. In the QCM-D experiments, a baseline signal in an aqueous buffer solution [10 mM Tris (pH 7.5) with appropriate NaCl concentration] was first established before bicelles or vesicles were added in the equivalent buffer solution. All solutions were added under continuous flow conditions using a peristaltic pump (Reglo Digital, Ismatec, Glattbrugg, Switzerland), and the flow rate was maintained at 50 μL/min, except during exchange steps. Measurement data were collected at multiple odd overtones by the Q-Soft software package (Biolin Scientific AB). The reported data were obtained at the 5th overtone and normalized according to the overtone number. Data processing was conducted using the Q-Tools (Biolin Scientific AB) and OriginPro (OriginLab, Northampton, MA) software programs.

Localized Surface Plasmon Resonance (LSPR). Ensemble-averaged LSPR measurements were performed in optical transmission mode using an Insplorion XNano instrument (Insplorion AB, Gothenburg, Sweden). The sensor chips (Insplorion AB) were composed of nonperiodic, noninteracting arrangements of gold nanodisks on a glass surface (surface coverage of ∼8%; each disk had an average height and diameter of 20 and 120 nm, respectively), and the entire array surface was sputter-coated with a thin silicon dioxide film (thickness ∼10 nm). Before each experiment, the sensor chips were thoroughly rinsed with 1 wt % sodium dodecyl sulfate (SDS) in water, water, and ethanol and dried with a stream of nitrogen gas, followed by oxygen plasma treatment. During the experiment, liquid samples were introduced using a peristaltic pump with a fixed flow rate of 50 μL/min. LSPR data were collected and analyzed using the Insplorer software package (Insplorion AB), and the data had a time resolution of 1 Hz. The extinction spectra were analyzed by high-order polynomial fitting to determine the LSPR peak position (formally calculated as the centroid position and denoted λ_{max}).[17]

Fluorescence Microscopy Imaging. The real-time adsorption of lipid bicelles and vesicles onto a glass surface was visualized by epifluorescence microscopy. For microscopy experiments, the lipid samples were prepared whereby the long-chain phospholipid fraction consisted of 99.5 DOPC lipid and 0.5 mol% Rh-PE lipid. The resulting lipid layers were imaged using a Nikon Eclipse Ti-E inverted microscope with a 60× oil-immersion objective (NA 1.49) and an Andor iXon3 897 EMCCD camera (Andor Technology, Belfast, Northern Ireland). The samples were illuminated by a TRITC (Rh-PE) filter set with a mercury lamp (Intenselight C-HGFIE; Nikon Corporation). Time-lapsed fluorescence micrographs of the lipid adsorption processes were recorded every 2 s.

RESULTS

Quartz Crystal Microbalance-Dissipation. We performed QCM-D experiments to investigate the effects of NaCl concentration on bicelle adsorption onto silicon dioxide surfaces. The sensor chips consisted of silicon dioxide-coated quartz crystals that exhibit piezoelectric behavior, whereby changes in the resonance frequency (Δf) and energy dissipation (ΔD) shifts due to lipid-related adsorption processes are monitored as a function of time.[18] The Δf and ΔD shifts reflect the mass and viscoelastic properties of the lipid adlayer, respectively, and thus provide insight into the amount and conformational properties of adsorbed lipid molecules. We performed equivalent experiments using DOPC/DHPC lipid bicelles and DOPC lipid vesicles that were prepared using identical protocols. For the experiments, the bicelles and vesicles were prepared in aqueous buffer with 150 mM NaCl and then diluted, immediately before the experiment, in an equivalent buffer with varying salt concentrations between 0 and 500 mM NaCl. In the context of osmotic pressure, the external NaCl concentration of 150 mM corresponds to isotonic condition (no osmotic pressure). If the bulk NaCl concentration is lower or higher than 150 mM, the osmotic pressure is negative or positive, respectively. The corresponding QCM-D measurement results are presented in Figure 2.

DOPC/DHPC Lipid Bicelles. Bicelle adsorption was observed to lead to SLB formation under all tested NaCl concentrations (Figure 2A−C). By analogy with vesicles,[18] the process occurs via the two-step scheme in which the adsorption of intact bicelles precedes SLB formation via bicelle rupture at a critical surface coverage. The final Δf and ΔD shifts were around −24 to −26 Hz and 0 to 0.1 × 10^{-6}, respectively, which are consistent with SLB formation.[6] Interestingly, in all cases, the Δf_{max} and ΔD_{max} shifts corresponding to the critical coverage were around −60 Hz and 3.0 × 10^{-6}, respectively. At 50 mM and greater NaCl concentrations, the time span until reaching the critical coverage was also similar; however, it took longer to reach a critical coverage of adsorbed bicelles at lower NaCl concentrations (0 and 25 mM NaCl conditions). Since PC lipid membranes have a slightly negative membrane surface potential and silicon dioxide surfaces are highly negatively charged under the experimental conditions, charge screening is reduced at lower NaCl concentrations, which in turn leads to greater electrostatic repulsion and weaker bicelle−substrate interactions. Under such conditions, bicelle adsorption appears to be reversible, and it can explain why the initial slope in the uptake is lower in this case. Interestingly, bicelle adsorption and SLB formation occurred under low salt conditions where small unilamellar vesicles typically adsorb but do not rupture.[7]

DOPC Lipid Vesicles. Depending on the NaCl concentration, vesicle adsorption resulted in SLB formation, moderate vesicle adsorption, or negligible vesicle adsorption (Figure 2D−F). At 50 mM and greater NaCl concentrations, two-step vesicle adsorption kinetics directly leading to SLB formation

DOI: 10.1021/acs.langmuir.9b01644
Langmuir 2019, 35, 10658−10666

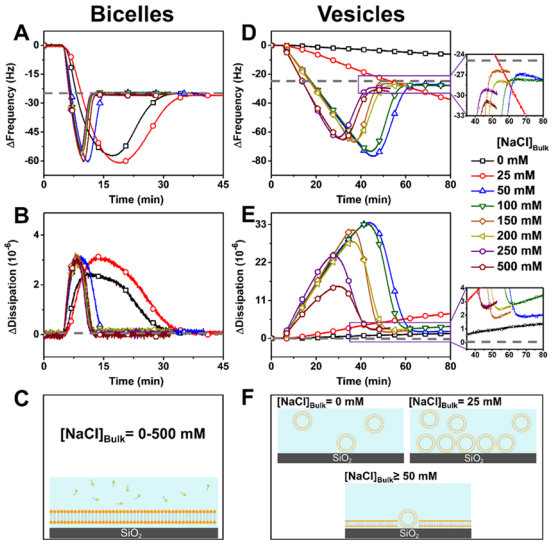

Figure 2. QCM-D monitoring of lipid bicelle and vesicle adsorption processes as a function of NaCl concentration. QCM-D data pertaining to lipid bicelle adsorption are presented for (A) frequency and (B) energy dissipation shifts as a function of time, along with (C) schematic illustration of the resulting formation process. (D–F) Corresponding data are shown for equivalent lipid vesicle adsorption experiments. Insets show magnified views of the final measurement responses for vesicle-mediated SLB formation. Baseline values were recorded in aqueous buffer solution before adding lipid bicelles or vesicles in equivalent buffer solution at t = 5 min.

was observed. Notably, the final Δf and ΔD shifts were around −26 to −32 Hz and 2.1×10^{-6} to 3.4×10^{-6}, respectively, which are indicative of incomplete SLB formation and the likely presence of some unruptured vesicles. With increasing NaCl concentration in this range (50–500 mM NaCl), the magnitudes of the Δf_{max} and ΔD_{max} shifts at the critical coverage became progressively smaller, shifting from around −75 to −60 Hz and 34×10^{-6} to 15×10^{-6}, respectively. This trend can be explained by how positive osmotic pressure conditions induce greater vesicle deformation (reflected in smaller Δf and ΔD shifts due to a thinner effective adlayer), whereas negative osmotic pressure conditions inhibit the deformation of adsorbed vesicles (reflected in larger Δf and ΔD shifts due to a thicker effective adlayer). By contrast, vesicle adsorption was only moderate and significantly slower in the 25 mM NaCl condition, and uptake was negligible in the 0 mM NaCl condition. Compared to the results obtained with small unilamellar vesicles, it is noteworthy that one-step adsorption kinetics with SLB formation just after adsorption is not observed at high positive osmotic pressure conditions, whereas vesicle adsorption appears less favorable at low NaCl concentrations. The latter result likely relates to the larger size of the vesicles used in this study, whereby the vesicle–substrate contact area would be larger and hence result in more repulsive interactions.

Localized Surface Plasmon Resonance. To corroborate the QCM-D data, we performed transmission-mode LSPR experiments to track real-time bicelle and vesicle adsorption and SLB formation onto silicon dioxide-coated sensor surfaces containing embedded gold nanodisk transducers.[19] Light illumination induces the coherent oscillation of electrons within the gold nanodisks, which creates an enhanced electromagnetic field near the sensor surface that is useful for detecting changes in the local refractive index, i.e., in response to bicelle and vesicle adsorption and/or SLB formation.[20,21] Experimentally, the optical extinction (absorption plus scattering) of transmitted light is detected and characterized by a maximum-extinction wavelength (λ_{max}) that is measured as a function of time. Typically, lipid-related adsorption processes induce a positive $\Delta\lambda_{max}$ shift because the refractive index of lipid molecules is larger than that of the solution media, and the local refractive index change influences the resonance conditions for maximum light extinction.[22]

The LSPR experiments were conducted using lipid bicelles and vesicles in 25, 150, and 300 mM bulk NaCl concentrations that are representative conditions for negative, zero, and positive osmotic pressure states, respectively (Figure 3). For

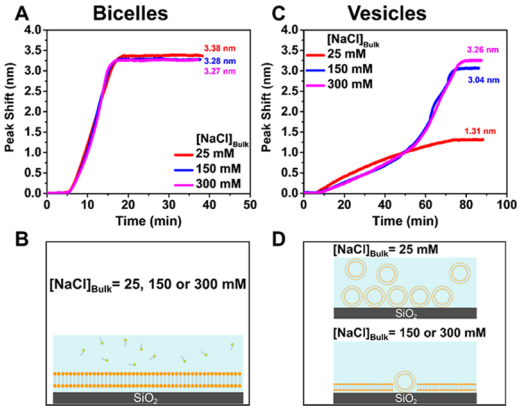

Figure 3. Wavelength-shift LSPR measurements for real-time optical characterization of lipid bicelle and vesicle adsorption processes. (A) DOPC/DHPC lipid bicelle adsorption data and (B) corresponding schematic illustration of the SLB formation process. (C) DOPC lipid vesicle adsorption data and (D) corresponding schematic illustration of the SLB formation or vesicle adsorption process at 25 (red), 150 (blue), and 300 (magenta) mM NaCl concentrations. Baseline values were recorded in aqueous buffer solution before adding lipid bicelles or vesicles in equivalent buffer solution at t = 5 min.

DOPC/DHPC lipid bicelles, successful SLB formation occurred in all three conditions, as indicated by similar time scales and nearly equivalent final $\Delta\lambda_{max}$ shifts of around 3.3 nm (Figure 3A,B). By contrast, the addition of DOPC lipid vesicles in 25 mM NaCl conditions led to monotonic adsorption, with a final $\Delta\lambda_{max}$ shift of ∼1.3 nm, which indicates weak adsorption of intact vesicles[23] (Figure 3C,D). On the other hand, SLB-like formation kinetics was observed for DOPC lipid vesicle addition in 150 and 300 mM NaCl conditions, with final $\Delta\lambda_{max}$ shifts of ∼3.0 and 3.2 nm, respectively. Notably, despite the same DOPC lipid concentration in the solution, the time scale of vesicle-mediated SLB formation was appreciably slower than that of bicelle-mediated SLB formation and exhibited more complex adsorption kinetics, suggesting incomplete formation.[24] Together, the LSPR data indicate that DOPC/DHPC lipid bicelles formed SLBs irrespective of the NaCl concentration, whereas DOPC lipid vesicles exhibited weak adsorption under negative osmotic pressure conditions and appeared to form incomplete SLBs under the other tested conditions. As such, the trends in the LSPR measurement data agree well with the trends observed in the QCM-D measurement data and led us to further investigate the morphological properties of the lipid adlayers formed in each case.

DOI: 10.1021/acs.langmuir.9b01644
Langmuir 2019, 35, 10658–10666

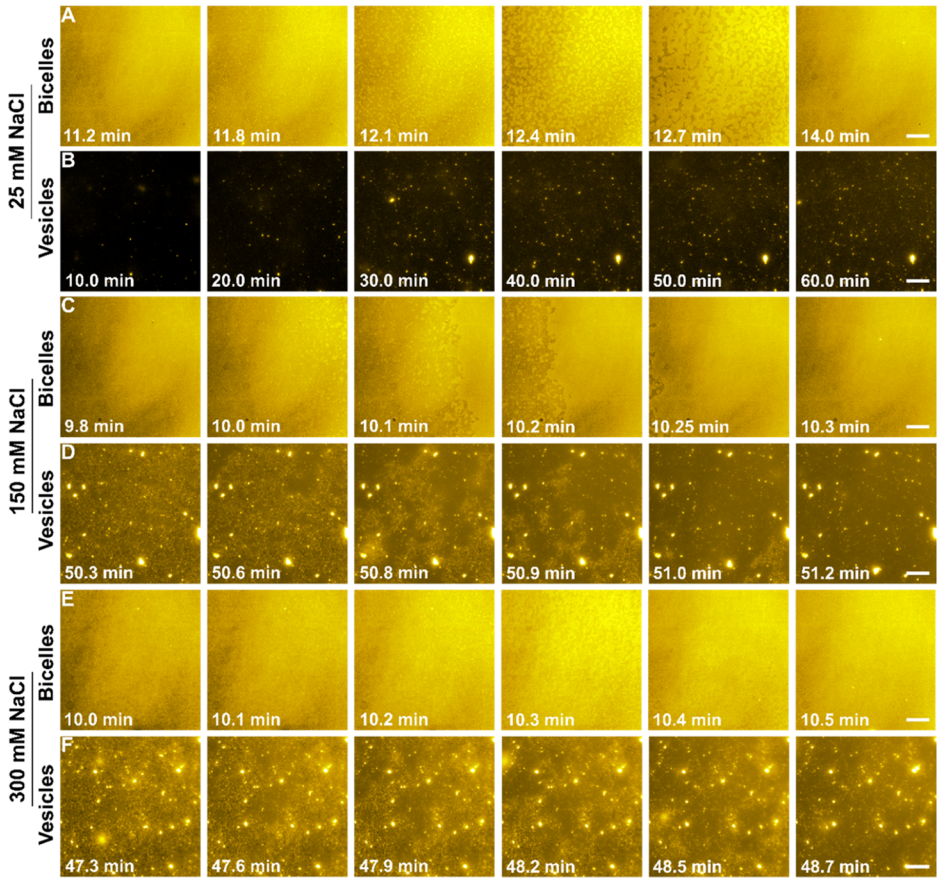

Figure 4. Time-lapsed fluorescence microscopy imaging of DOPC/DHPC lipid bicelle and DOPC lipid vesicle adsorption at different NaCl concentrations. The data correspond to (A) bicelle and (B) vesicle addition in 25 mM NaCl salt condition, (C) bicelle and (D) vesicle addition in 150 mM NaCl salt condition, and (E) bicelle and (F) vesicle addition in 300 mM NaCl salt condition. Bicelles or vesicles were added onto the glass surface at t = 0 min. Contrast adjustment was applied to visualize adsorbing lipid species in each snapshot series. All scale bars are 20 μm.

Time-Lapsed Fluorescence Microscopy Imaging. We conducted time-lapsed epifluorescence microscopy imaging to directly observe lipid bicelle and vesicle adsorption onto a glass surface. The lipid bicelles and vesicles contained a minor fraction of fluorescently labeled lipid molecules for visualization purposes, and the samples were prepared in 25, 150, and 300 mM bulk NaCl concentrations that are representative conditions for negative, zero and positive osmotic pressure states, respectively. The samples were injected into a microfluidic chamber under flow-through conditions, and the initial injection time was defined as t = 0 min. In cases of complete or incomplete SLB formation, the presented micrographs start when the critical surface coverage of adsorbed lipid bicelles or vesicles was reached. In other cases where lipid adsorption was negligible, a sampling of representative micrographs from across the measurement time span is provided. SLB formation was also confirmed by FRAP measurements (see Figure S1). The details of each experimental series are presented in Figure 4 and discussed below.

25 mM NaCl. Bicelles adsorbed quickly and a critical surface coverage was reached after around 11.2 min, followed by the appearance of small, bright spots corresponding to bicelle fusion and subsequent SLB formation (Figure 4A). Bilayer propagation occurred rapidly within 2 min, resulting in complete SLB formation with uniform fluorescence properties. By contrast, vesicles adsorbed more gradually, as indicated by a growing number of bright dots corresponding to individual, adsorbed vesicles (Figure 4B). Adsorbed vesicles remained intact and did not rupture; thus, no critical surface coverage was reached and SLB formation did not occur in this case. The relatively low salt concentration likely impeded vesicle rupture due to limited screening of moderately repulsive vesicle–substrate interactions along with inducing a negative osmotic pressure to counteract substrate-mediated vesicle deformation.[7]

150 mM NaCl. Bicelle adsorption was rapid again, and the critical surface coverage was reached after around 9.8 min. Bilayer propagation was appreciably quicker in this case, occurring within 0.5 min and resulting in the formation of a complete SLB (Figure 4C). Compared to the 25 mM NaCl case, vesicle adsorption also occurred to a greater extent and there was a critical surface coverage of adsorbed vesicles at around 50 min (Figure 4D). Vesicle fusion was marked by a discernible change in fluorescence properties of the adlayer, shifting from the granular appearance of individual vesicles to a more uniform fluorescence that is typically associated with an SLB. There were also many bright spots that did not vanish upon SLB formation and are indicative of unruptured vesicles, as has been seen before with large vesicles.[25] Thus, vesicle adsorption led to incomplete SLB formation, including the presence of unruptured vesicles.

300 mM NaCl. Bicelle adsorption occurred on a similar time scale to the 150 mM NaCl case, and a critical surface coverage of adsorbed bicelles was reached at around 10 min (Figure 4E). Bilayer propagation proceeded even more quickly

DOI: 10.1021/acs.langmuir.9b01644
Langmuir 2019, 35, 10658–10666

afterward, and the SLB formation process was complete within 0.2 min. Likewise, vesicles exhibited similar adsorption behavior to the 150 mM NaCl case (Figure 4F). The critical surface coverage was reached around 47 min and bilayer propagation events were detected based on the change in the fluorescence intensity profile, although there were still unruptured vesicles within the formed SLB.

DISCUSSION

We have already outlined various mechanistic aspects of SLB formation via bicelle and vesicle adsorption and rupture and briefly discussed some of the features of the corresponding QCM-D and LSPR adsorption kinetics. As noted above, there was general agreement between the QCM-D and LSPR data. Here, the discussion is extended to articulate the similarities and differences in the adsorption behavior of adsorbed bicelles and vesicles and to point out trends along with some distinctions that are observed in the QCM-D and LSPR data.

Kinetics of the SLB Formation Process. The QCM-D adsorption kinetics support that the influence of NaCl concentration on adsorption and rupture is largely negligible in the case of bicelles and appreciable in the case of vesicles. For zwitterionic lipid vesicles, interpretation of the vesicle-mediated SLB formation on silicon dioxide surfaces has long been shown to be possible in the framework of a kinetic model that includes three channels of vesicle rupture or, more specifically, (i) spontaneous rupture of individual vesicles, (ii) vesicle fusion with subsequent rupture, and (iii) rupture induced by already formed lipid membrane islands near the island boundaries.[26−28] Channels (ii) and (iii) often dominate. In particular, vesicle rupture starts via channel (ii) [or (i)] after reaching a critical surface coverage of adsorbed vesicles, and then the SLB front rapidly propagates via channel (iii). The critical coverage associated approximately with the maximum QCM-frequency shift, Δf_{max}, is close to saturation because otherwise the kinetic conditions for propagation are not fulfilled. The drop in the absolute value of the QCM-D frequency shift after reaching the maximum is expected to be related primarily to the loss of trapped solvent after vesicle rupture.

The kinetics of vesicle attachment is controlled by diffusion up until reaching Δf_{max}, and under the flow conditions, the surface number concentration of vesicles can be represented as

$$N \propto D^{2/3}\rho_m t/4\pi R_v^2 \quad (1)$$

where ρ_m, $4\pi R_v^2$, and D are the lipid mass density, vesicle surface area (R_v is the radius), and vesicle diffusion coefficient in solution, respectively.[16,27] The deformation of adsorbed vesicles on silicon dioxide surfaces appears to take place primarily near the vesicle−support contact, whereas the vesicle radius remains close to R_v.[7] Thus, the vesicle coverage scales as

$$\theta \propto N\pi R_v^2 \propto D^{2/3}\rho_m t/4 \quad (2)$$

where πR_v^2 is the cross-sectional area, and accordingly, the time interval from the onset of attachment until reaching Δf_{max} scales as

$$\Delta t_* \propto 4/\rho_m D^{2/3} \quad (3)$$

For the diffusion coefficient, the hydrodynamics yield $1/R_v$. Using this expression, we have

$$\Delta t_* \propto 4R_v^{2/3}/\rho_m \quad (4)$$

In the present experiments with DOPC/DHPC lipid bicelles, the total lipid concentration in solution was low (0.155 mM) and the q-value was relatively low (0.25) as well. In this case, the DHPC lipids are in excess and the solution is expected to contain relatively large DOPC/DHPC lipid bicelles along with small DHPC micelles or monomers.[14] The attachment of small DHPC micelles, if present, is reversible and, at the low lipid concentration under consideration, their uptake is negligible (see the Supporting Information in ref 14). Thus, the SLB formation kinetics we present are presumably related to attachment and rupture of DOPC/DHPC lipid bicelles. Qualitatively, the shape of these kinetics is similar to those observed in the case of DOPC lipid vesicles, and a reasonable conjecture is to consider that, in the DOPC/DHPC case, the process also occurs via reaching the critical coverage, which is close to saturation and subsequent rupture. Quantitatively, however, the DOPC/DHPC and DOPC lipid adsorption kinetics are quite different, and these distinctions can be used to clarify the specifics of the DOPC/DHPC case.

An important point is that the DOPC/DHPC and DOPC lipid adsorption kinetics were measured at a fixed DOPC lipid concentration (0.031 mM). According to dynamic light scattering experiments, the DOPC vesicle size distribution had a mean diameter of around 300 nm, whereas the DOPC/DHPC bicelle size distribution had a mean diameter of around 470 nm. Another important point is that the molecular sizes of DOPC and DHPC lipids are quite different, and accordingly, their appreciable mixing in vesicles with relatively large curvature or in the flat parts of bicelles is energetically not favorable. In particular, the DOPC/DHPC lipid structures are known to contain DHPC lipids primarily near the rim, and integrally in the bicelles of the size of interest, the contribution of these lipids to the bicellar surface area or volume is small. The flat part of bicelles may also contain DHPC lipids (from this perspective, one can consider that the bicelles are in the "mixed" state[29]), but their concentration is low. Thus, we can consider that the DOPC/DHPC lipid bicelles are composed primarily of DOPC lipids. In this case, the surface number concentration of the bicellar structures can be represented as

$$N \propto D^{2/3}\rho_m t/\pi R_b^2 \quad (5)$$

where ρ_m, πR_b^2, and D are the DOPC lipid mass density, bicelle surface area (R_b is the radius), and bicelle diffusion coefficient in solution, respectively. To roughly estimate the surface coverage by bicelles, one can consider that they are located primarily so that their flat part is oriented along the surface and, accordingly, we have

$$\theta \propto N\pi R_b^2 \propto D^{2/3}\rho_m t \quad (6)$$

where πR_b^2 is the cross-sectional area, and

$$\Delta t_* \propto 1/\rho_m D^{2/3} \propto R_b^{2/3}/\rho_m \quad (7)$$

Due to the absence of numerical factor 4 and with the sizes of our bicelles and vesicles (470 nm versus 300 nm hydrodynamic diameter) and equal DOPC lipid concentrations in the solution, this expression predicts a few times shorter time scale compared to that predicted by expression (4). This difference is in qualitative agreement with what was observed in our experiments, supporting that physically the initial phases of the adsorption kinetics of the DOPC/DHPC lipid bicelles and DOPC lipid vesicles are similar.

DOI: 10.1021/acs.langmuir.9b01644
Langmuir 2019, 35, 10658−10666

The important difference in the mechanisms of SLB formation via vesicle and bicelle rupture is related to the nature of the contact between these lipid nanostructures and the underlying solid support. In the former case, the critical condition for the propagation of the SLB front is reached when the mass of intact adsorbed vesicles is slightly larger than that needed to form an SLB.[26−28] In the case of bicelles fully contacting the support, the area of an SLB spot that can be formed after bicelle rupture is nearly equal to the bicelle−support contact area, and front propagation is hardly possible if the surface is covered only by such bicelles. This means that the whole process occurs apparently in the same fashion as in the case of vesicles and likely involves bicelles attached perpendicularly or under an angle with respect to the support, i.e., bicelles contacting the support via their edge containing DHPC lipids. Under such circumstances, the drop in the absolute value of the QCM-D frequency shift after reaching a maximum appears to be related primarily to detachment of an appreciable fraction of bicelles attached perpendicularly or under an angle with respect to the support and partly to the loss of the solvent trapped by such bicelles.

The difference indicated above can be used to explain the qualitative difference in the behavior of the LSPR signal after the onset of SLB formation via bicelle or vesicle rupture (cf. Figure 2A,D). In the case of vesicles, their rupture results in an appreciable increase in the fraction of the surface covered by an SLB, and accordingly, the LSPR signal rapidly increases after the onset of rupture. By contrast, in the case of bicelles, the contribution of bicelles, oriented along the surface, to the LSPR signal does not change, and the contribution of bicelles, oriented perpendicularly to the surface, to the LSPR signal is relatively small and comparable to that of the lipids released after the rupture of these bicelles (this can be confirmed by estimates of the corresponding contributions based on the equations presented in ref 30), and accordingly, there is no rapid increase in the LSPR signal after the onset of bicelle rupture.

Influence of NaCl Concentration on SLB Formation Kinetics. The time intervals to reach the maximum frequency shift at critical coverage Δf_{max} (Δt_*) and to reach $0.5\Delta f_{max}$ from the critical coverage, i.e., rupture rate ($\Delta t_{1/2}$) as a function of bulk NaCl concentration during adsorption of DOCP/DHPC lipid bicelles and DOPC lipid vesicles, were compared to examine the influence of this concentration on the kinetics (Figure 5A,B). As discussed above, the time intervals Δt_* of bicelles in all adsorption cases were approximately 4 times shorter than those of vesicles. The linear dependence of Δt_* on NaCl concentration was observed only in the low-concentration (negative osmotic pressure) regime for bicelles. However, Δt_* decreased with increasing osmotic pressure for vesicles in cases with two-step adsorption kinetics where the critical coverage was reached, i.e., in 50 mM NaCl and above. The dependence of $\Delta t_{1/2}$ on NaCl concentration is similar to that of Δt_* for bicelles; the rupture rate increased with increasing NaCl concentration only in the range of 0−100 mM, above which $\Delta t_{1/2}$ remained constant. For vesicles, the influence of NaCl concentration on $\Delta t_{1/2}$ was not as pronounced as that on Δt_*, albeit similar. In terms of SLB formation, bicelle adsorption led to the formation of complete SLBs in all cases with no dependence on NaCl concentration, whereas vesicles formed incomplete SLBs only in the cases of 50−500 mM NaCl concentrations. Below, we further discuss the mechanistic aspects of the NaCl concentration effect.

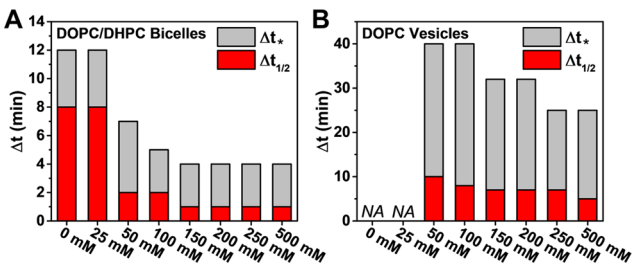

Figure 5. Time scales of QCM-D adsorption kinetics (Δt_* and $\Delta t_{1/2}$) versus NaCl concentration for (A) DOPC/DHPC bicelle adsorption and (B) DOPC vesicle adsorption. "NA" denotes "not applicable" in cases where SLB formation did not occur.

As already noted in the Introduction, the influence of bulk NaCl concentration on the kinetics under consideration results from (i) the corresponding osmotic pressure and (ii) electrostatic contribution to the interaction of bicelles or vesicles with the silicon dioxide surface. In the case of zwitterionic lipid vesicles on silicon dioxide, both these factors work in the same direction.[7] In particular, a greater positive osmotic pressure (with increasing NaCl concentration outside of the vesicles) facilitates vesicle deformation as well as vesicle rupture. The silicon dioxide surface and vesicles are both negatively charged. Although the charge concentration is low in both cases, the screening of the corresponding Coulomb interaction with increasing NaCl concentration is favorable for vesicle adsorption and rupture. In the present experiments with DOPC lipid vesicles, in line with these arguments, we observed significant rupture resulting in lipid adlayers that are close-to-complete SLBs at appreciable NaCl concentrations, whereas at low NaCl concentrations, rupture did not occur. The deformation of vesicles in solution also influences the vesicle diffusion coefficient, and accordingly, Δt_* is influenced as well, but this effect is relatively weak[31] and can be neglected as it has been done in our estimations above (eqs 4 and 7).

In the DOPC/DHPC lipid case, as already noticed, the effect of the NaCl-related osmotic pressure on the shape of disklike bicelles and accordingly on their adsorption and rupture is expected to be negligible because the disklike structure is relatively compact. This type of bicellar structure has been confirmed by various biophysical techniques.[9,32−35] Furthermore, the effect of the NaCl-related charge screening is not expected to be dramatic because, as already noticed, the charge concentrations of both the silicon dioxide surface and vesicle surface are low. In agreement with these arguments, our experiment indicates that the effect of NaCl on bicelle-mediated SLB formation is weak and SLB can be formed irrespective of the NaCl concentration. In future work, it will also be interesting to explore other ion-related effects on bicelle adsorption pathways. For example, monovalent and divalent cations can bind to phospholipid headgroups and influence lipid−substrate interactions either directly (via bridging interactions) or indirectly (via charge screening), whereas anions are expected to have more indirect effects and typically compensate for the positive charge of counter-cations.[36]

In summary, the experimental results obtained using the QCM-D and LSPR techniques revealed many interesting similarities and difference in bicelle- versus vesicle-mediated SLB formation. These techniques are shown to be highly

DOI: 10.1021/acs.langmuir.9b01644
Langmuir 2019, 35, 10658−10666

complementary, and their integrated use provides new insights into the process of bicelle adsorption and rupture. In general, the QCM-D and LSPR results were mutually supporting; however, one related aspect remains open for discussion. In particular, the QCM-D results indicate that the initial slope of the vesicle adsorption kinetics depends on the NaCl concentration (cf. Figure 2D), and at relatively high NaCl concentrations, this can be attributed to the deformation of adsorbed vesicles due to osmotic pressure effects. A similar feature might be expected, but was not observed, in the LSPR results (cf. Figure 3C). A likely explanation is that there are correlations in the location of adsorbed vesicles (which are relatively large) and 120 nm diameter LSPR gold disk transducers, thus reinforcing that the different surface-sensitive measurement techniques have particular advantages and the combination of these techniques is useful for unraveling the details of how NaCl concentration affects bicelle-mediated SLB formation.

Looking forward, our results demonstrate that bicelles appear to be robust and versatile tools for SLB fabrication in different environmental conditions and thus may be useful for various interfacial science and engineering applications.

■ ASSOCIATED CONTENT

Supporting Information

The Supporting Information is available free of charge on the ACS Publications website at DOI: 10.1021/acs.langmuir.9b01644.

Fluorescence recovery after photobleaching (FRAP); time-lapsed FRAP micrographs for lipid adlayers formed in aqueous buffers containing 25, 150, or 300 mM bulk NaCl concentrations (Figure S1) (PDF)

■ AUTHOR INFORMATION

Corresponding Author

*E-mail: njcho@ntu.edu.sg.

ORCID

Joshua A. Jackman: 0000-0002-1800-8102

Soohyun Park: 0000-0003-3261-7585

Nam-Joon Cho: 0000-0002-8692-8955

Notes

The authors declare no competing financial interest.

■ ACKNOWLEDGMENTS

This work was supported by the National Research Foundation of Singapore through a Competitive Research Programme grant (NRF-CRP10-2012-07) and a Proof-of-Concept grant (NRF2015NRF-POC0001-19) as well as through the Center for Precision Biology at Nanyang Technological University. Additional support was provided by the Creative Materials Discovery Program through the National Research Foundation of Korea funded by the Ministry of Science, ICT and Future Planning (NRF-2016M3D1A1024098).

■ REFERENCES

(1) Hardy, G. J.; Nayak, R.; Zauscher, S. Model Cell Membranes: Techniques to Form Complex Biomimetic Supported Lipid Bilayers via Vesicle Fusion. *Curr. Opin. Colloid Interface Sci.* **2013**, *18*, 448−458.

(2) Mashaghi, A.; Mashaghi, S.; Reviakine, I.; Heeren, R. M.; Sandoghdar, V.; Bonn, M. Label-Free Characterization of Biomembranes: From Structure to Dynamics. *Chem. Soc. Rev.* **2014**, *43*, 887−900.

(3) Komiyama, M.; Yoshimoto, K.; Sisido, M.; Ariga, K. Chemistry Can Make Strict and Fuzzy Controls for Bio-Systems: DNA Nanoarchitectonics and Cell-Macromolecular Nanoarchitectonics. *Bull. Chem. Soc. Jpn.* **2017**, *90*, 967−1004.

(4) Ariga, K.; Mori, T.; Li, J. Langmuir Nanoarchitectonics from Basic to Frontier. *Langmuir* **2019**, *35*, 3585−3599.

(5) Richter, R. P.; Bérat, R.; Brisson, A. R. Formation of Solid-Supported Lipid Bilayers: An Integrated View. *Langmuir* **2006**, *22*, 3497−3505.

(6) Keller, C.; Kasemo, B. Surface Specific Kinetics of Lipid Vesicle Adsorption Measured with a Quartz Crystal Microbalance. *Biophys. J.* **1998**, *75*, 1397−1402.

(7) Jackman, J. A.; Choi, J.-H.; Zhdanov, V. P.; Cho, N.-J. Influence of Osmotic Pressure on Adhesion of Lipid Vesicles to Solid Supports. *Langmuir* **2013**, *29*, 11375−11384.

(8) Tabaei, S. R.; Choi, J.-H.; Haw Zan, G.; Zhdanov, V. P.; Cho, N.-J. Solvent-Assisted Lipid Bilayer Formation on Silicon Dioxide and Gold. *Langmuir* **2014**, *30*, 10363−10373.

(9) van Dam, L.; Karlsson, G.; Edwards, K. Direct Observation and Characterization of DMPC/DHPC Aggregates under Conditions Relevant for Biological Solution NMR. *Biochim. Biophys. Acta, Biomembr.* **2004**, *1664*, 241−256.

(10) Dürr, U. H. N.; Soong, R.; Ramamoorthy, A. When Detergent Meets Bilayer: Birth and Coming of Age of Lipid Bicelles. *Prog. Nucl. Magn. Reson. Spectrosc.* **2013**, *69*, 1.

(11) Zeineldin, R.; Last, J. A.; Slade, A. L.; Ista, L. K.; Bisong, P.; O'Brien, M. J.; Brueck, S.; Sasaki, D. Y.; Lopez, G. P. Using Bicellar Mixtures to Form Supported and Suspended Lipid Bilayers on Silicon Chips. *Langmuir* **2006**, *22*, 8163−8168.

(12) Tabaei, S. R.; Jönsson, P.; Brändén, M.; Höök, F. Self-Assembly Formation of Multiple DNA-Tethered Lipid Bilayers. *J. Struct. Biol.* **2009**, *168*, 200−206.

(13) Morigaki, K.; Kimura, S.; Okada, K.; Kawasaki, T.; Kawasaki, K. Formation of Substrate-Supported Membranes from Mixtures of Long-and Short-Chain Phospholipids. *Langmuir* **2012**, *28*, 9649−9655.

(14) Kolahdouzan, K.; Jackman, J. A.; Yoon, B. K.; Kim, M. C.; Johal, M. S.; Cho, N.-J. Optimizing the Formation of Supported Lipid Bilayers from Bicellar Mixtures. *Langmuir* **2017**, *33*, 5052−5064.

(15) Sut, T. N.; Jackman, J. A.; Cho, N.-J. Understanding How Membrane Surface Charge Influences Lipid Bicelle Adsorption onto Oxide Surfaces. *Langmuir* **2019**, *35*, 8436−8444.

(16) Jackman, J. A.; Zan, G. H.; Zhao, Z.; Cho, N.-J. Contribution of the Hydration Force to Vesicle Adhesion on Titanium Oxide. *Langmuir* **2014**, *30*, 5368−5372.

(17) Dahlin, A. B.; Tegenfeldt, J. O.; Höök, F. Improving the Instrumental Resolution of Sensors Based on Localized Surface Plasmon Resonance. *Anal. Chem.* **2006**, *78*, 4416−4423.

(18) Cho, N.-J.; Frank, C. W.; Kasemo, B.; Höök, F. Quartz Crystal Microbalance with Dissipation Monitoring of Supported Lipid Bilayers on Various Substrates. *Nat. Protoc.* **2010**, *5*, 1096.

(19) Zan, G. H.; Jackman, J. A.; Kim, S. O.; Cho, N. J. Controlling Lipid Membrane Architecture for Tunable Nanoplasmonic Biosensing. *Small* **2014**, *10*, 4828−4832.

(20) Willets, K. A.; Van Duyne, R. P. Localized Surface Plasmon Resonance Spectroscopy and Sensing. *Annu. Rev. Phys. Chem.* **2007**, *58*, 267−297.

(21) Jackman, J. A.; Ferhan, A. R.; Cho, N.-J. Nanoplasmonic Sensors for Biointerfacial Science. *Chem. Soc. Rev.* **2017**, *46*, 3615−3660.

(22) Anker, J. N.; Hall, W. P.; Lyandres, O.; Shah, N. C.; Zhao, J.; Van Duyne, R. P. Biosensing with Plasmonic Nanosensors. *Nat. Mater.* **2008**, *7*, 442−453.

(23) Jackman, J. A.; Yorulmaz Avsar, S.; Ferhan, A. R.; Li, D.; Park, J. H.; Zhdanov, V. P.; Cho, N.-J. Quantitative Profiling of Nanoscale Liposome Deformation by a Localized Surface Plasmon Resonance Sensor. *Anal. Chem.* **2017**, *89*, 1102−1109.

DOI: 10.1021/acs.langmuir.9b01644
Langmuir 2019, 35, 10658−10666

(24) Jackman, J. A.; Kim, M. C.; Zhdanov, V. P.; Cho, N.-J. Relationship between Vesicle Size and Steric Hindrance Influences Vesicle Rupture on Solid Supports. *Phys. Chem. Chem. Phys.* **2016**, *18*, 3065−3072.
(25) Kim, M. C.; Gunnarsson, A.; Tabaei, S. R.; Höök, F.; Cho, N.-J. Supported Lipid Bilayer Repair Mediated by AH Peptide. *Phys. Chem. Chem. Phys.* **2016**, *18*, 3040−3047.
(26) Keller, C.; Glasmästar, K.; Zhdanov, V.; Kasemo, B. Formation of Supported Membranes from Vesicles. *Phys. Rev. Lett.* **2000**, *84*, 5443.
(27) Zhdanov, V.; Keller, C.; Glasmästar, K.; Kasemo, B. Simulation of Adsorption Kinetics of Lipid Vesicles. *J. Chem. Phys.* **2000**, *112*, 900−909.
(28) Mapar, M.; Jõemetsa, S.; Pace, H.; Zhdanov, V. P.; Agnarsson, Br.; Höök, F. Spatiotemporal Kinetics of Supported Lipid Bilayer Formation on Glass Via Vesicle Adsorption and Rupture. *J. Phys. Chem. Lett.* **2018**, *9*, 5143−5149.
(29) Nieh, M.-P.; Raghunathan, V. A.; Kline, S. R.; Harroun, T. A.; Huang, C.-Y.; Pencer, J.; Katsaras, J. Spontaneously Formed Unilamellar Vesicles with Path-Dependent Size Distribution. *Langmuir* **2005**, *21*, 6656−6661.
(30) Oh, E.; Jackman, J. A.; Yorulmaz, S.; Zhdanov, V. P.; Lee, H.; Cho, N.-J. Contribution of Temperature to Deformation of Adsorbed Vesicles Studied by Nanoplasmonic Biosensing. *Langmuir* **2015**, *31*, 771−781.
(31) Jackman, J. A.; Goh, H. Z.; Zhdanov, V. P.; Knoll, W.; Cho, N.-J. Deciphering How Pore Formation Causes Strain-Induced Membrane Lysis of Lipid Vesicles. *J. Am. Chem. Soc.* **2016**, *138*, 1406−1413.
(32) Gaemers, S.; Bax, A. Morphology of Three Lyotropic Liquid Crystalline Biological NMR Media Studied by Translational Diffusion Anisotropy. *J. Am. Chem. Soc.* **2001**, *123*, 12343−12352.
(33) Triba, M. N.; Devaux, P. F.; Warschawski, D. E. Effects of Lipid Chain Length and Unsaturation on Bicelles Stability. A Phosphorus NMR Study. *Biophys. J.* **2006**, *91*, 1357−1367.
(34) Nieh, M.-P.; Raghunathan, V.; Glinka, C. J.; Harroun, T. A.; Pabst, G.; Katsaras, J. Magnetically Alignable Phase of Phospholipid "Bicelle" Mixtures Is a Chiral Nematic Made up of Wormlike Micelles. *Langmuir* **2004**, *20*, 7893−7897.
(35) Rodríguez, G.; Cócera, M.; Rubio, L.; López-Iglesias, C.; Pons, R.; de la Maza, A.; López, O. A Unique Bicellar Nanosystem Combining Two Effects on Stratum Corneum Lipids. *Mol. Pharmaceutics* **2012**, *9*, 482−491.
(36) Vácha, R.; Siu, S. W.; Petrov, M.; Böckmann, R. A.; Barucha-Kraszewska, J.; Jurkiewicz, P.; Hof, M.; Berkowitz, M. L.; Jungwirth, P. Effects of Alkali Cations and Halide Anions on the DOPC Lipid Membrane. *J. Phys. Chem. A* **2009**, *113*, 7235−7243.

DOI: 10.1021/acs.langmuir.9b01644
Langmuir 2019, 35, 10658−10666